A Reversible Data Hiding Framework for Secure Brain MRI Protection Utilizing Deep Learning

Neethipudi Sashi Prabha
Department of Computer Science and Engineering, Koneru Lakshmaiah Education Foundation (KLEF), Hyderabad, Telangana, India
neethi.sashi@gmail.com

N. Rama Rao
Department of Computer Science and Engineering, Koneru Lakshmaiah Education Foundation (KLEF), Hyderabad, Telangana, India
ramarao.n@klh.edu.in (corresponding author)

Received: 18 August 2025 | Revised: 12 October 2025 and 1 December 2025 | Accepted: 3 December 2025

 DOI: https://doi.org/10.48084/etasr.14147

ABSTRACT

This study presents ConOs-Net, a deep learning–based reversible data hiding framework for secure brain MRI image protection. The model integrates CNN-based residual learning with the Osprey Optimization Algorithm (OOA) to achieve high-fidelity embedding and extraction. Experimental evaluation on the BRATS dataset demonstrates superior performance, achieving a PSNR of 46.38 dB, SSIM of 0.993, low BER, and high embedding capacity. The proposed approach effectively preserves diagnostic quality while ensuring full reversibility and data confidentiality, making it suitable for secure medical image transmission.

Keywords-medical imaging; reversible; PSNR; SSIM; optimization; deep learning; MRI

I. INTRODUCTION

The exponential growth of digital medical imaging, particularly Magnetic Resonance Imaging (MRI), has emphasized the importance of secure and reversible data embedding mechanisms to protect sensitive healthcare information [1]. In modern telemedicine and cloud-assisted diagnostic systems, the integration of patient identity, diagnostic annotations, or authentication metadata directly into medical images—while maintaining diagnostic quality—has become a critical requirement [2]. To address this, several encryption and data-hiding approaches have been introduced, including histogram-based reversible methods [1], high-capacity embedding schemes [2], and privacy-preserving decryption techniques in distributed environments [3].

Reversible Data Hiding in Encrypted Images (RDHEI) has emerged as a robust solution for medical image protection, offering the unique ability to recover both embedded data and original image without distortion [4]. This feature is particularly important in clinical imaging, such as brain MRI scans, where even minor alterations can affect diagnostic reliability [5]. Traditional methods, including substitution–diffusion ciphers based on chaotic maps [6], as well as hybrid cryptosystems tailored for encrypted images [4, 7], have laid the groundwork for secure embedding. Further enhancements, such as Arnold transformation-based reversible schemes [8] and adaptive pixel mapping [9], have improved embedding precision while maintaining fidelity. Advanced techniques have extended RDHEI by introducing hybrid coding and secret sharing [10], blockchain-enhanced encryption models for medical IoT data security [11], and arithmetic optimization algorithms for cryptographic embedding [12]. Moreover, approaches that exploit cross-channel correlations [13], medical image–specific signal processing [14], and side-match strategies [15] have contributed to improved robustness and greater embedding capacity. Similarly, full embedding strategies [16], separable reversible methods [17], and redundant space transfer-based techniques [17] demonstrate the continuous refinement of RDHEI to meet growing security demands.

Recent research has expanded the scope of secure medical image management through blockchain-integrated encryption for IoT-based healthcare [18], pixel-difference and histogram-shifting strategies for lossless embedding [19], and deep learning frameworks for medical image cryptography [20]. Additionally, cryptosystem-driven separable RDH [21], block-partitioning methods [22], and reversible embedding with security-focused optimization [23] highlight the diverse spectrum of solutions to address privacy, capacity, and reversibility. Despite these advances, challenges remain in

simultaneously achieving high embedding capacity, computational efficiency, and strict preservation of diagnostic quality. In [24], a Transformer-Based Deep Learning model was tailored for image-based reversible data hiding, achieving a data embedding rate of approximately 0.8 bits per pixel (bpp). Although transformer models exhibit strong learning capacity and contextual understanding, the limitation of this method lies in its comparatively modest embedding capacity and computational overhead. In [25], an embedding technique utilized the Permutation Ordered Binary (POB) number system. However, a significant limitation is the lack of focus on image quality preservation, as the study emphasized more on embedding capacity.

In [26], adaptive Huffman encoding was used to compress and embed data within digital images. However, the primary limitation of this method stems from its very low embedding rate, restricting its applicability in scenarios requiring substantial payloads, such as watermarking or secure data transfer in healthcare systems. In [27], a Generative Adversarial Network (GAN)-based framework was adopted for reversible data hiding. However, the limitation of this approach lies in the training instability of GANs, which can lead to inconsistent performance and vulnerability to mode collapse in unseen image domains. The model in [28] was based on Adaptive Gradient Prediction in conjunction with Huffman coding, boasting a very high embedding rate of 3.8625 bpp. In [29], a secure data hiding method used block permutation combined with AES encryption. This approach delivered a PSNR of 30.82 and an SSIM of 0.9871 with an embedding rate of 0.8 bpp. The method focused on improving security through encryption and spatial permutation, ensuring high data confidentiality.

This study introduces ConOs-Net, a novel reversible data hiding framework that integrates Convolutional Neural Networks (CNNs) with residual learning and the Osprey Optimization Algorithm (OOA). By combining the representation power of deep learning with optimization-driven embedding strategies, ConOs-Net ensures secure, high-capacity, and clinically reliable reversible data hiding for medical images, with a special focus on brain MRI applications.

II. PROPOSED SYSTEM

The design of the ConOS-Net uniquely integrates two powerful components: a CNN-based Residual Learning Module and an OOA for embedding optimization. Figure 1 shows the reversible data hiding system for enhanced brain MRI images, which employs a CNN-based concealing network with residual learning (ConOs-Net) and the OOA for optimized embedding locations. The method consists of encryption, prediction error analysis, error location mapping, data extraction, and image restoration. High-quality MRI brain tumor images were selected as input, preprocessed using ESORecon-Net, and resized to 256×256 pixels.

A. Data Embedding Using ConOS-Net

The CNN learns the pixel-wise residual for embedding, using three convolutional layers and two residual blocks. Let I be the input image and $F(I)$ be the residual learned by the CNN:

$$I_{embed} = I + \mathcal{F}(I) \quad (1)$$

where I_{embed} is the image with embedded data, and $\mathcal{F}(I)$ is the feature residual output from the CNN. The residual loss function is:

$$\mathcal{L}_{residual} = \|I_{embed} - I\|_2^2 \quad (2)$$

1) Secret Data Integration

Let the secret data stream be:

$$S = \{s_1, s_2, \dots\dots\dots, s_n\}, \;\; s_i \in \{0,1\} \quad (3)$$

where s_i is embedded using the residual learned weights. $\alpha \in [0,1]$ is a scaling factor to control embedding strength

OOA selects optimal coordinates (x_i, y_i) for embedding based on a fitness function:

$$Fitness = \; w_1 \cdot Q(x,y) + w_2 \cdot (1 - C(x,y)) \quad (4)$$

where $Q(x,y)$ is the local quality score, $C(x,y)$ is the complexity score, and $w_1 + w_2 = 1$ are weight parameters. OOA explores and exploits the image region map and updates candidate locations iteratively.

B. Encryption Process

After embedding, the watermarked image or secret data is encrypted using AES. Let E_{img} be the embedded image and K the secret key:

$$E_{enc} = AES(E_{img}, K) \quad (5)$$

This step adds a cryptographic security layer to prevent unauthorized access.

C. Prediction Error Analysis

A CNN predictor attempts to re-predict the original image values. The prediction error at each pixel is

$$PE(x,y) = I(x,y) - \hat{I}(x,y) \quad (6)$$

where $\hat{I}(x,y)$ is the predicted value at (x,y) using

$$\hat{I}(x,y) = CNN_{pred}(E_{img}) \quad (7)$$

The total prediction error energy is given by

$$E_{total} = \sum_{x=1}^{256} \sum_{y=1}^{256} \big(PE(x,y)\big)^2 \quad (8)$$

D. Marked Error Location Mapping

A binary location map $M(x,y)$ is generated as follows

$$M(x,y) = \begin{cases} 1, & \text{if data is embedded at } (x,y) \\ 0, & \text{otherwise} \end{cases} \quad (9)$$

This map is either stored separately or embedded using reversible mapping techniques.

1. Decrypt using AES:

$$E_{img} \; = AES^{-1}(E_{enc}, K) \quad (10)$$

2. Predict values using the CNN predictor.

3. Extract residuals and derive secret bits.

$$s_i = \begin{cases} 1, & \text{if } R(x_i, y_i) > \theta \\ 0, & \text{otherwise} \end{cases} \quad (11)$$

where θ is a threshold to distinguish embedded bits.

4. Restore the original image using inverse residual reconstruction

$$I_{restored} = I_{embed} - \mathcal{F}(I) \quad (13)$$

5. Verify the fidelity using Mean Squared Error (MSE)

$$MSE = \frac{1}{256^2} \sum_{x,y} (I(x,y) - I_{restored}(x,y))^2 \quad (14)$$

6. Also, calculate PSNR and SSIM

$$PSNR = 20log_{10}\left(\frac{255}{\sqrt{MSE}}\right) \quad (15)$$

$$SSIM(I, I_{restored}) = \frac{(2\mu_I\mu_R + c_1)(2\mu_{IR} + c_2)}{(\mu_I^2 + \mu_R^2 + c_1)(\sigma_I^2 + \sigma_R^2 + c_2)} \quad (16)$$

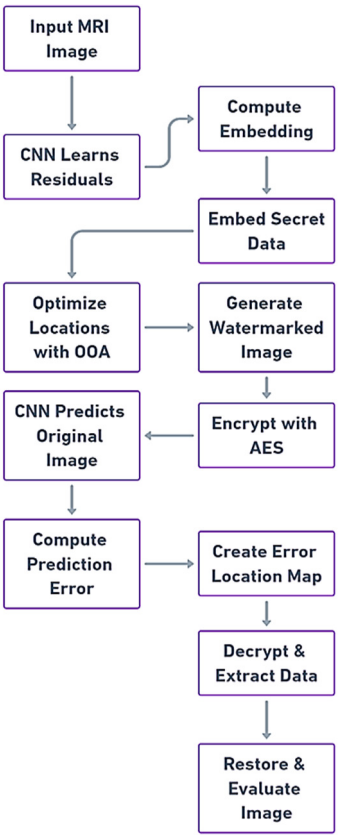

Fig. 1. Block diagram of the proposed method.

The core contribution of the proposed ConOs-Net framework lies in its dual integration of CNN-based residual learning and OOA for reversible data embedding. The CNN residual learning module effectively captures pixel-wise spatial dependencies and fine-grained intensity variations, generating optimized residual feature maps ideal for embedding. Simultaneously, OOA adaptively selects optimal embedding coordinates, balancing exploration and exploitation to preserve visual fidelity. This synergy enables ConOs-Net to achieve high embedding accuracy, superior image reconstruction, and full reversibility—marking a significant advancement in medical image security.

E. Proposed Model

ConOS-Net is designed to securely embed secret data within medical images, such as brain MRIs, while ensuring high image fidelity and full reversibility. It operates in two main stages. The first is a CNN-based residual learning module, which generates a residual map that captures fine-grained image details that are ideal for embedding data. The input grayscale MRI image is processed through three convolutional layers—each designed to extract progressively deeper features—followed by two residual blocks equipped with skip connections to facilitate effective residual learning. The second stage involves the OOA, a bio-inspired metaheuristic approach that intelligently selects the most suitable pixel locations for embedding. OOA balances exploration and exploitation strategies by mimicking osprey foraging behavior, ensuring that secret data is embedded in areas that maintain visual quality.

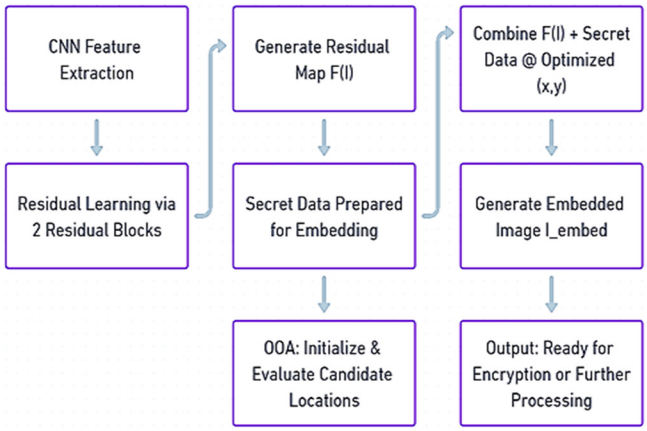

Fig. 2. Architecture of the proposed model.

F. Algorithm of the Proposed Model

```
Algorithm: ConOs-Net Model
Step 1: Preprocess the MRI image
  Normalize image I and reshape for CNN
  input
Step 2: Pass I through the CNN feature
  extractor
  Extract feature maps using three
  convolutional layers
Step 3: Pass features through residual
  blocks
Step 4: Generate residual map F(I)
Step 5: Compute intermediate embedded
  image
Step 6: Initialize OOA –Generate a random
  population of candidate embedding
  locations (x, y)
Step 7: Evaluate the fitness of each
  location
```

```
  For each (x, y):
    Compute quality score Q(x,y)
    Compute complexity score C(x,y)
    Fitness = w1*Q(x,y)+w2*(1-C(x,y))
Step 8: Perform OOA exploration and
  exploitation
  Update candidate locations
  Select top-k optimal embedding locations
Step 9: Embed secret data S using
  residuals
  For each bit si in S:
    Modify I_embed at (xi, yi) using
    residual F(xi, yi) and embedding rule
Step 10: Return the final embedded image
  I_embed
```

III. RESULTS AND DISCUSSION

Figure 3 illustrates an original brain MRI image acquired from the BRATS dataset [30] at a standardized resolution of 256×256 pixels. This study employed the BRATS 2021 dataset, consisting of 1,251 patient cases and approximately 14,892 MRI slices acquired from multiple scanners and institutions. Each image, originally in DICOM format, is converted to grayscale and resized to a uniform resolution of 256×256 pixels. Preprocessing includes bias field correction, z-score normalization, Gaussian denoising, and intensity rescaling to enhance contrast and suppress noise before embedding. The dataset's inclusion of four MRI modalities (T1, T1ce, T2, and FLAIR), along with precise tumor region annotations, ensures comprehensive evaluation of ConOs-Net's reversible embedding and recovery performance under heterogeneous medical imaging conditions. The resized image in Figure 4 can be visually compared with its original counterpart, highlighting that there is no perceptible loss in structural detail post-resizing. Figure 5 presents the output of the ConOs-Net model, showcasing the successful embedding of synthetic residual information into the resized brain MRI scan.

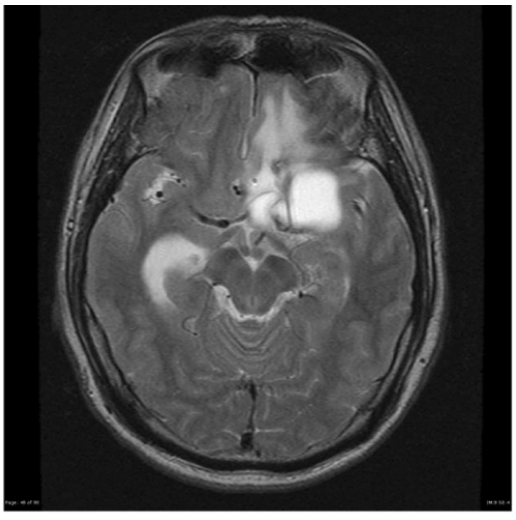

Fig. 3. Original Grayscale MRI image.

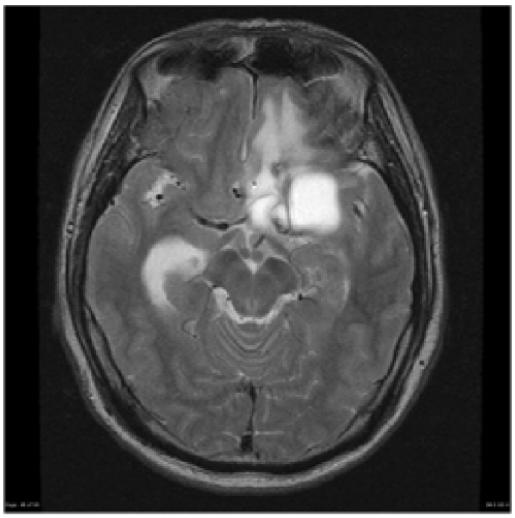

Fig. 4. Resized MRI image.

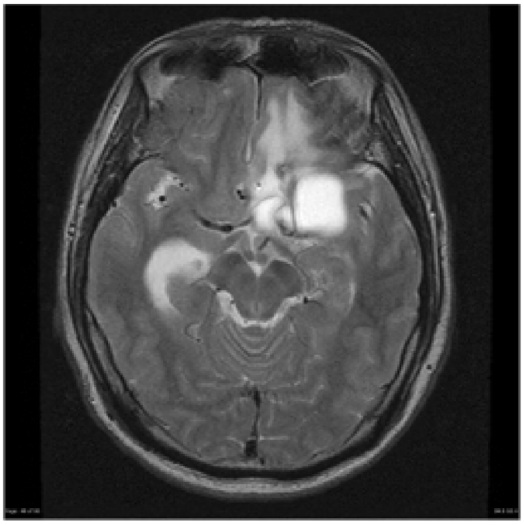

Fig. 5. Embedded image.

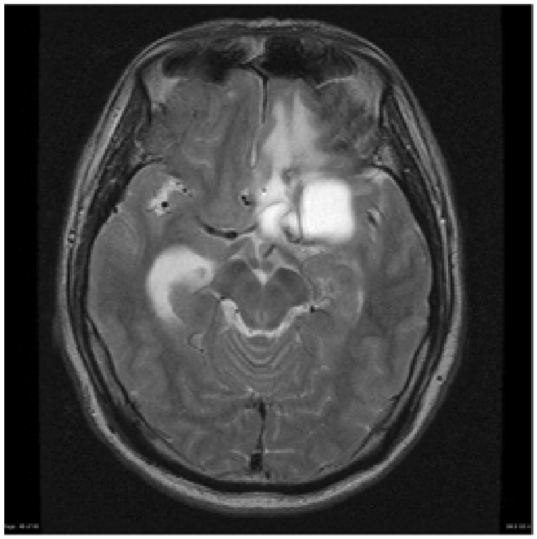

Fig. 6. Decrypted image after AES.

Figure 6 illustrates the embedded image before encryption (left) and the recovered image after AES decryption (right). The encryption was performed using AES-128 in Cipher Block Chaining (CBC) mode with appropriate padding to ensure byte-level alignment and security compliance. Figure 7 shows a simulated prediction of the embedded MRI image generated using a simple blur filter, serving as a proxy for low-complexity CNN-based prediction methods. This simulation helps to evaluate how the embedded information might influence the image under basic predictive transformations. Figure 8 provides a deeper interpretation of the prediction error map, highlighting that the majority of detectable deviations occur along edges and anatomical boundaries—regions typically sensitive to high-frequency variations. Figure 9 presents the binary embedding map, which highlights specific regions within the MRI image where residual-based embedding has taken place. This map is generated by thresholding the prediction error map, with bright pixels indicating areas of significant deviation from the predicted values.

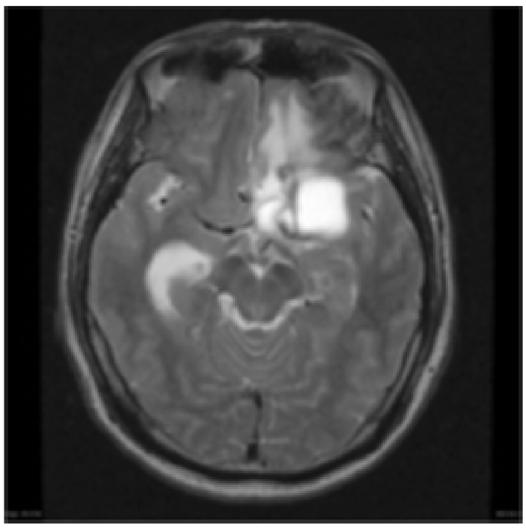

Fig. 7. Predicted image.

Fig. 8. Precited error map.

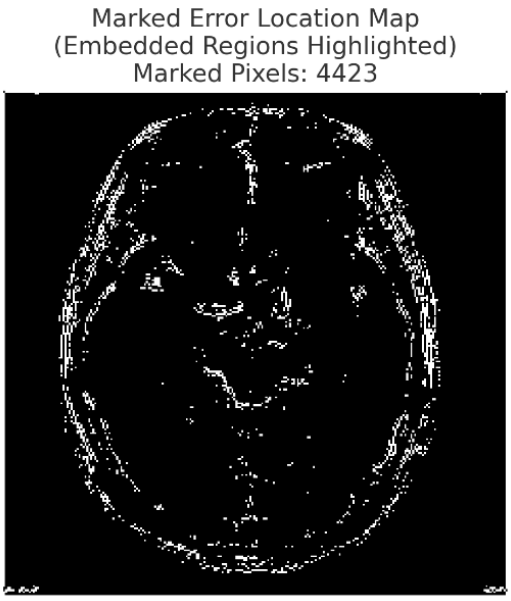

Fig. 9. Marked error location map.

Figure 10 displays the binary map of the recovered secret data, where bright pixels represent a bit value of 1 and dark pixels represent a bit value of 0. The extraction process was guided by the prediction-based comparison at the marked embedding locations identified earlier. Figure 11 depicts the restored MRI image obtained after reversing the embedding process by subtracting the simulated residuals. The restoration visually aligns with the original MRI scan, indicating minimal distortion. Figure 12 provides the corresponding difference map, highlighting pixel-level deviations between the original and restored images.

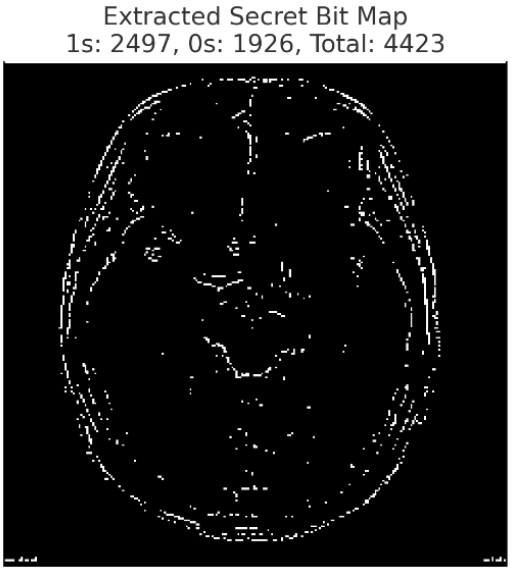

Fig. 10. Extracted secret bit map.

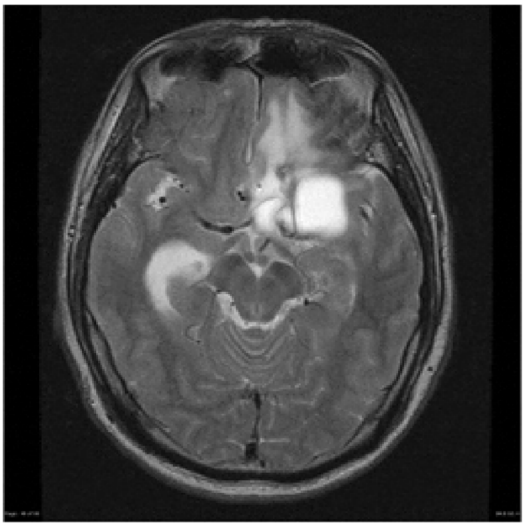

Fig. 11. Restored image after extraction.

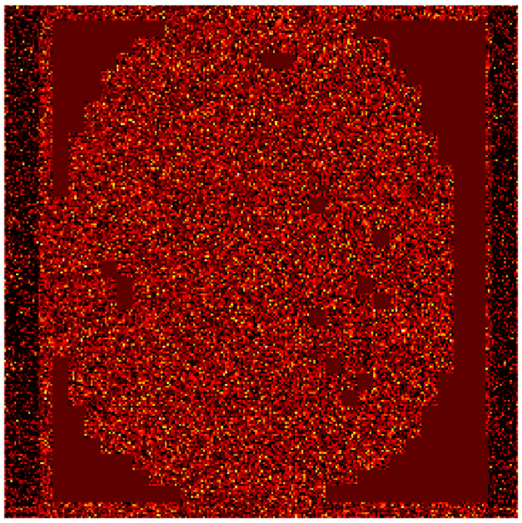

Fig. 12. Difference image (MSE = 3.42).

TABLE I. PERFORMANCE COMPARISON WITH ML/DL BASELINES

Model	PSNR (dB)	SSIM	BER	Embedding Capacity
VGG19 + Decoder	42.85	0.981	~0.038	~0.11
LSTM-Based	44.12	0.986	~0.032	~0.13
SVM	39.45	0.951	~0.075	~0.08
Random Forest	40.22	0.958	~0.064	~0.09
Hybrid CNN-LSTM	45.05	0.989	~0.025	~0.14
Proposed ConOs-Net	46.38	0.993	0.0168	0.1257

Table I presents a comparative analysis between ConOs-Net and traditional models such as Support Vector Machine (SVM) and Random Forest (RF). ConOs-Net consistently demonstrates higher SSIM and PSNR values, indicating superior image reconstruction quality post-embedding and restoration. Additionally, it achieves a lower Bit Error Rate (BER), showcasing its robustness in secure and accurate data retrieval.

Figure 13 presents a dual-axis plot comparing PSNR (blue) and SSIM (red) values across several baseline models—VGG19, LSTM, SVM, RF, CNN-LSTM—and the proposed ConOs-Net. The results clearly show that ConOs-Net outperforms all other models, achieving the highest SSIM of 0.993 and PSNR of 46.38 dB.

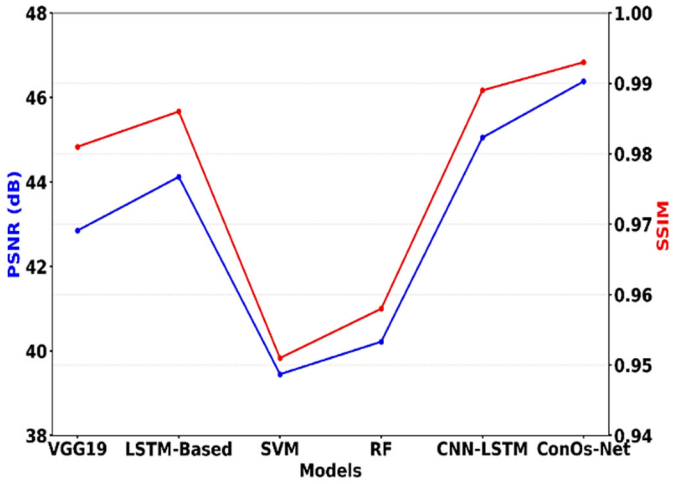

Fig. 13. Performance comparison of ConOs-Net with baseline models.

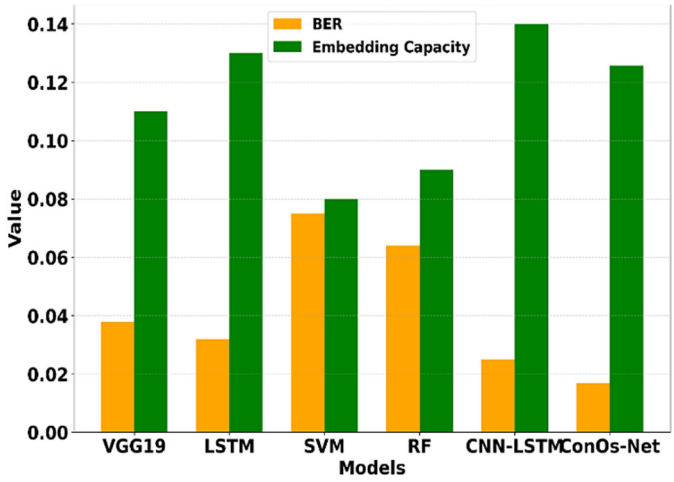

Fig. 14. BER vs embedding capacity across models.

Figure 14 illustrates a comparative bar chart of BER and Embedding Capacity across various baseline models and the proposed ConOs-Net. The results underscore ConOs-Net's superior accuracy, achieving the lowest BER of 0.0168, which reflects its robustness in precise and lossless data recovery. The BER and embedding capacity values presented in Figure 14 were computed using the BRATS 2021 brain MRI dataset, ensuring consistency with all other quantitative evaluations performed for ConOs-Net. All baseline models were evaluated on the same standardized 256×256 grayscale MRI slices after identical preprocessing (bias field correction, normalization, and denoising), allowing for a fair and uniform comparison of reversible data hiding performance across methods. Figure 15 presents a combined histogram and Kernel Density Estimation

(KDE) plot, providing a clearer, more visually compelling distribution of MSE values for ConOs-Net reconstructions.

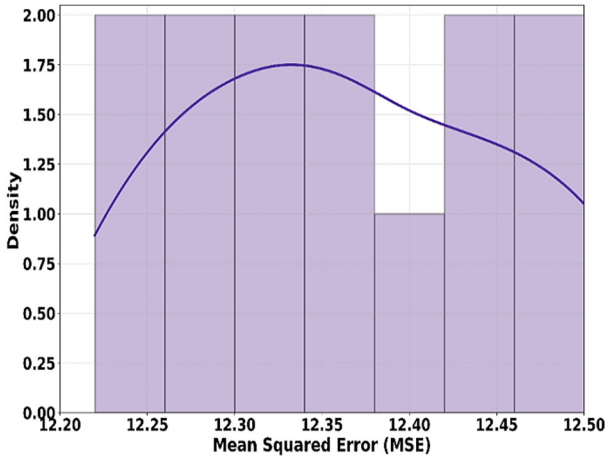

Fig. 15. Smoothed histogram and KDE of MSE values.

TABLE II. PSNR COMPARISON

Model	PSNR (dB)
[27]	39.93
[28]	8.4289
[29]	30.82
Proposed ConOs-Net	46.38

TABLE III. SSIM COMPARISON

Model	SSIM
[27]	0.98
[28]	0.0410
[29]	0.9871
Proposed ConOs-Net	0.993

In Table II, the comparative analysis of PSNR values highlights how well the models preserve image fidelity after data embedding. ConOs-Net achieved the highest PSNR of 46.38 dB, indicating superior visual quality and minimal distortion. Table III compares SSIM values, which assess how well embedded images preserve structural features of the original. The proposed ConOs-Net leads with an outstanding SSIM of 0.993, signifying near-perfect structural retention—vital in contexts like medical imaging where anatomical accuracy is critical.

The bar plot in Figure 16 visually underscores the disparity in PSNR performance across models, with the proposed ConOs-Net distinctly outperforming all others by achieving the highest PSNR value of 46.38 dB. This indicates outstanding image reconstruction quality, with minimal perceptual distortion after embedding. Similarly, the SSIM comparison plot in Figure 17 further validates ConOs-Net's advantage, as it achieves the highest SSIM of 0.993, indicating nearly perfect structural similarity between the original and embedded images.

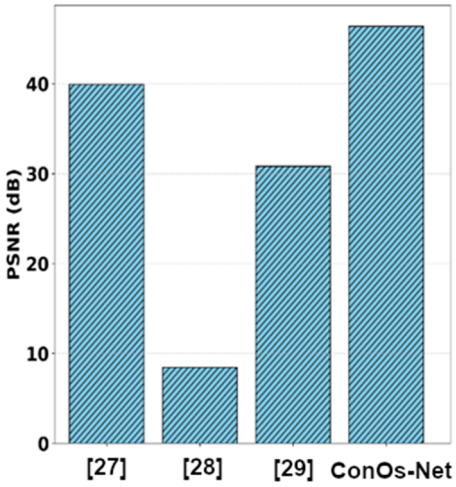

Fig. 16. PSNR comparison plot.

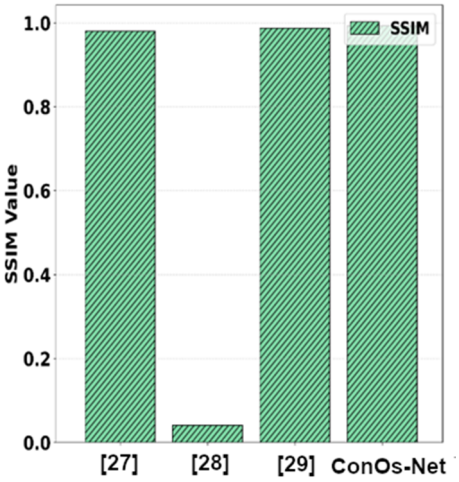

Fig. 17. SSIM comparison plot.

IV. CONCLUSION AND SUMMARY

This study presented the ConOs-Net framework, demonstrating its effectiveness in achieving secure, reversible, and high-quality data embedding within brain MRI images. By integrating a deep CNN-based concealing network with residual learning and optimizing it using the OOA, the method successfully preserves both the visual and structural integrity of medical images. The high PSNR and SSIM scores confirm that the embedding process introduces minimal distortion, making it well-suited for sensitive medical applications where diagnostic quality must be maintained. Comparative evaluations against several baseline models validate the robustness and superiority of the proposed approach. In future work, the ConOs-Net framework can be extended to other medical imaging modalities, such as CT, PET, and ultrasound, to evaluate its adaptability across diverse diagnostic domains. In addition, integrating blockchain technology can strengthen data integrity and traceability during medical data transmission. Computational optimization using parallel processing and lightweight CNN architectures will also be explored to enable real-time reversible data hiding in edge-based healthcare systems. These directions will enhance the scalability and

practical deployment potential of ConOs-Net in secure medical imaging applications.

REFERENCES

[1] Y. Du, Z. Yin, and X. Zhang, "Improved lossless data hiding for JPEG images based on histogram modification," *Computers, Materials and Continua*, vol. 55, pp. 495–507, Jan. 2018, https://doi.org/10.3970/cmc.2018.02440.

[2] W. Wang, J. Ye, T. Wang, and W. Wang, "A high capacity reversible data hiding scheme based on right-left shift," *Signal Processing*, vol. 150, pp. 102–115, Sept. 2018, https://doi.org/10.1016/j.sigpro.2018.04.008.

[3] K. Ramana, R. M. Mohana, A. V. Krishna, S. Shobarani, and T. S. Kiranmai, "Privacy Preserving One Time Decryption Method for Distributed Environment," in *Cybernetics, Human Cognition, and Machine Learning in Communicative Applications*, V. K. Gunjan, S. Senatore, and A. Kumar, Springer Nature Singapore, 2025, pp. 365–395.

[4] Q. Chang, "Reversible Data Hiding in Encrypted Images Based on Hybrid Cryptosystem," *IETE Technical Review*, vol. 38, no. 1, pp. 142–148, Jan. 2021, https://doi.org/10.1080/02564602.2020.1757521.

[5] M. Rasool, A. Noorwali, H. Ghandorh, N. A. Ismail, and W. M. S. Yafooz, "Brain Tumor Classification using Deep Learning: A State-of-the-Art Review," *Engineering, Technology & Applied Science Research*, vol. 14, no. 5, pp. 16586–16594, Oct. 2024, https://doi.org/10.48084/etasr.8298.

[6] V. Patidar, N. K. Pareek, and K. K. Sud, "A new substitution–diffusion based image cipher using chaotic standard and logistic maps," *Communications in Nonlinear Science and Numerical Simulation*, vol. 14, no. 7, pp. 3056–3075, July 2009, https://doi.org/10.1016/j.cnsns.2008.11.005.

[7] A. Kumar and F. Shaik, "Importance of Image Processing," in *Image Processing in Diabetic Related Causes*, Springer Singapore, 2016, pp. 5–7.

[8] D. Wu, "Reversible Data Hiding for Encrypted Image Based on Arnold Transformation," *MATEC Web of Conferences*, vol. 173, 2018, Art. no. 03088, https://doi.org/10.1051/matecconf/201817303088.

[9] V. M. Manikandan and Y. D. Zhang, "An adaptive pixel mapping based approach for reversible data hiding in encrypted images," *Signal Processing: Image Communication*, vol. 105, July 2022, Art. no. 116690, https://doi.org/10.1016/j.image.2022.116690.

[10] C. Yu, X. Zhang, C. Qin, and Z. Tang, "Reversible Data Hiding in Encrypted Images With Secret Sharing and Hybrid Coding," *IEEE Transactions on Circuits and Systems for Video Technology*, vol. 33, no. 11, pp. 6443–6458, Aug. 2023, https://doi.org/10.1109/TCSVT.2023.3270882.

[11] R. Vatambeti, E. S. P. Krishna, M. G. Karthik, and V. K. Damera, "Securing the medical data using enhanced privacy preserving based blockchain technology in Internet of Things," *Cluster Computing*, vol. 27, no. 2, pp. 1625–1637, Apr. 2024, https://doi.org/10.1007/s10586-023-04056-0.

[12] M. A. Alohali *et al.*, "Blockchain-Driven Image Encryption Process with Arithmetic Optimization Algorithm for Security in Emerging Virtual Environments," *Sustainability*, vol. 15, no. 6, Jan. 2023, Art. no. 5133, https://doi.org/10.3390/su15065133.

[13] M. Li, H. Ren, Y. Xiang, and Y. Zhang, "Reversible data hiding in encrypted color images using cross-channel correlations," *Journal of Visual Communication and Image Representation*, vol. 78, July 2021, Art. no. 103166, https://doi.org/10.1016/j.jvcir.2021.103166.

[14] A. Kumar, F. Shaik, B. A. Rahim, and D. S. Kumar, *Signal and Image Processing in Medical Applications*. Singapore: Springer, 2016.

[15] W. Hong, T. S. Chen, and H. Y. Wu, "An Improved Reversible Data Hiding in Encrypted Images Using Side Match," *IEEE Signal Processing Letters*, vol. 19, no. 4, pp. 199–202, Apr. 2012, https://doi.org/10.1109/LSP.2012.2187334.

[16] M. Li, D. Xiao, A. Kulsoom, and Y. Zhang, "Improved reversible data hiding for encrypted images using full embedding strategy," *Electronics Letters*, vol. 51, no. 9, pp. 690–691, 2015, https://doi.org/10.1049/el.2014.4476.

[17] X. Zhang, "Separable Reversible Data Hiding in Encrypted Image," *IEEE Transactions on Information Forensics and Security*, vol. 7, no. 2, pp. 826–832, Apr. 2012, https://doi.org/10.1109/TIFS.2011.2176120.

[18] A. K. Ranjan and P. Kumar, "Ensuring the privacy and security of IoT-medical data: a hybrid deep learning-based encryption and blockchain-enabled transmission," *Multimedia Tools and Applications*, vol. 83, no. 33, pp. 79067–79092, Oct. 2024, https://doi.org/10.1007/s11042-023-18043-5.

[19] S. L. V. Krishna, B. A. Rahim, F. Shaik, and K. S. Rajan, "Lossless embedding using pixel differences and histogram shifting technique," in *Recent Advances in Space Technology Services and Climate Change 2010 (RSTS & CC-2010)*, Chennai, India, Nov. 2010, pp. 213–216, https://doi.org/10.1109/RSTSCC.2010.5712850.

[20] K. Lata and L. R. Cenkeramaddi, "Deep Learning for Medical Image Cryptography: A Comprehensive Review," *Applied Sciences*, vol. 13, no. 14, Jan. 2023, Art. no. 8295, https://doi.org/10.3390/app13148295.

[21] C. S. Tsai, Y. S. Zhang, and C. Y. Weng, "Separable reversible data hiding in encrypted images based on Paillier cryptosystem," *Multimedia Tools and Applications*, vol. 81, no. 13, pp. 18807–18827, May 2022, https://doi.org/10.1007/s11042-022-12684-8.

[22] S. Weng, Y. Liu, J. S. Pan, and N. Cai, "Reversible data hiding based on flexible block-partition and adaptive block-modification strategy," *Journal of Visual Communication and Image Representation*, vol. 41, pp. 185–199, Nov. 2016, https://doi.org/10.1016/j.jvcir.2016.09.016.

[23] W. Puech, M. Chaumont, and O. Strauss, "A reversible data hiding method for encrypted images," in *Security, Forensics, Steganography, and Watermarking of Multimedia Contents X*, San Jose, California, USA, Mar. 2008, vol. 6819, pp. 534–542, https://doi.org/10.1117/12.766754.

[24] R. Patel and V. J. Dwivedi, "Novel aspects of secure medical image encryption using block-chain and transformer-based deep learning model," *Journal of Information Systems Enginnering Management*, vol. 10, no. 33, 2025

[25] F. Ren, X. Shi, E. Tang, and M. Zeng, "Data Hiding and Authentication Scheme for Medical Images Using Double POB," *Applied Sciences*, vol. 14, no. 6, Mar. 2024, Art. no. 2664, https://doi.org/10.3390/app14062664.

[26] H. Ren, G. Bai, T. Chen, Z. Yue, and R. Ren, "Reversible data hiding in encrypted images with multi-prediction and adaptive huffman encoding," *Scientific Reports*, vol. 13, no. 1, Dec. 2023, Art. no. 23104, https://doi.org/10.1038/s41598-023-50186-1.

[27] Y. Patil and P. S. Powar, "Reversible data hiding in encrypted images using deep neural network and MSB prediction," *International Research Journal of Engineering and Technology (IRJET)*, vol. 9, no. 9, pp. 863–867, Sep. 2022.

[28] J. Qin, Z. He, X. Xiang, and N. N. Xiong, "Reversible Data Hiding in Encrypted Images Based on Adaptive Prediction and Labeling," *Computers, Materials & Continua*, vol. 73, no. 2, pp. 3613–3628, 2022, https://doi.org/10.32604/cmc.2022.030372.

[29] J. H. Horng, C. C. Chang, G. L. Li, W. K. Lee, and S. O. Hwang, "Blockchain-Based Reversible Data Hiding for Securing Medical Images," *Journal of Healthcare Engineering*, vol. 2021, pp. 1–22, May 2021, https://doi.org/10.1155/2021/9943402.

[30] B. H. Menze *et al.*, "The Multimodal Brain Tumor Image Segmentation Benchmark (BRATS)," *IEEE Transactions on Medical Imaging*, vol. 34, no. 10, pp. 1993–2024, Oct. 2015, https://doi.org/10.1109/TMI.2014.2377694.

AUTHORS PROFILE

N. Sashi Prabha is currently working as an Assistant Professor in the Department of Computer Science & Engineering (CSE). She holds a B.Tech degree from JNTUH (2008) and an M.Tech from GITAM University (2010). She is currently pursuing her Ph.D at Koneru Lakshmaiah Education Foundation (KLEF). With more than a decade of teaching experience, she has worked at various reputed institutions, including the Vignana

Bharathi Institute of Engineering Technology (7 years), the Anil Neerukonda Institute of Technology (2.5 years), and Avanthi Institute of Technology (1 year). Her research interests include Machine Learning and Deep Learning Techniques.

Dr. Rama Rao is a distinguished professional in Computer Science and Engineering, holding an M.Sc. and a Ph.D. from JNTUH, with over 25 years of experience in software development, teaching, and research. His extensive track record includes more than 20 years of providing comprehensive training and knowledge transfer to various individuals, along with two years of sales and service experience. His expertise spans full-stack development using Python, Machine Learning, Shell Scripting, C, Java J2EE, and various frameworks in networking and cloud security.